Research on Chemical Intermediates (2022) 48:5155–5168
https://doi.org/10.1007/s11164-022-04857-9

Methane-to-methanol conversion and power co-generation on palladium: nickel supported on antimony tin oxide catalysts in a polymeric electrolyte reactor-fuel cell (PER-FC)

Jessica F. Coelho[1] · Nivaldo G. P. Filho[1] · Isabely M. Gutierrez[1] · Camila M. Godoi[1] · Paulo V. R. Gomes[1] · Priscilla J. Zambiazi[1] · Rodrigo F. B. de Souza[1] · Almir O. Neto[1]

Received: 16 August 2022 / Accepted: 11 October 2022 / Published online: 19 October 2022

Abstract

The use of palladium nickel catalysts with different compositions supported metal oxides, such as $Sb_2O_5{\cdot}SnO_2$ (ATO) catalyst combinations were employed to convert the methane-to-methanol in mild conditions using a fuel cell polymer electrolyte reactor. The catalysts used for the conversion of methane to methanol were characterized by XRD and observed the phases of ATO, the face-centered cubic structure of the Pd and Ni phases. All nanoparticles have a mean size between 9 and 12 nm as measured by TEM images. The products obtained from the methane oxidation, such as methanol and formate, were monitored using FT-IR spectroscopy to qualify the products formation, while High-Performance Liquid Chromatography was used to quantify them. In these studies, it was observed that as the electrical potential of the reactor increases, the generation of products decreases. The best results for the conversion of methane into methanol and energy co-generation were obtained from $Pd_{50}Ni_{50}$/ATO.

Keywords Methane conversion · PdNi/ATO · Reactor-type fuel cell · Methanol production

✉ Almir O. Neto
aolivei@usp.br

[1] Instituto de Pesquisas Energéticas e Nucleares, IPEN-CNEN/SP, Cidade Universitária, Av. Prof. Lineu Prestes, 2242, São Paulo, SP 05508-900, Brazil

Introduction

The warming caused by anthropogenic emissions will persist for centuries, and consequently, long-term changes in the climate system will be continuous and irreversible. However, achieving and maintaining net-zero global anthropogenic emissions and decarbonization would be sufficient to keep global warming below 2 °C. In this sense, different mitigation strategies can achieve net emission reductions through combinations of technologies and innovations. In this vein, the global methane pledge, announced at COP26, aims to reduce methane emissions by 30% by 2030 compared to 2020 levels [1].

The conversion of methane into higher energy products such as methanol is a great challenge because it contributes both to the environment and to the economy. However, it is not a simple task because this hydrocarbon showing high stability and its products have substantial reactivity, such as methanol, formaldehyde, or formic acid [2]. Thus, the selectivity and production of methanol from methane oxidation in excellent yields are dependent on the catalyst and the reaction system. Under these conditions, it is necessary to ensure that the reaction system needs to activate the methane under mild conditions and also controls the reaction path of the activated methane.

Using fuel cell technology, such as a polymer electrolyte membrane fuel cell (PEMFC), methane can be partially oxidized and converted into more useful chemicals. In these devices, the reaction products can be selected by adjusting the applied work potential. Thus, selectivity for methanol can be achieved [3]. The partial oxidation of methane in a polymer electrolyte reactor-fuel cell type (PER-FC) occurs by the activation of water, which results in the generation of reactive oxygenated species, which are capable of activating the C–H bond of methane [4], as explained in Eqs. 1–3, by a non-faradaic pathway [4–6].

$$H_2O_{(liq)} + M \rightarrow MOH \tag{1}$$

$$MOH \rightarrow M + OH- \text{ and/or } \cdot OH \tag{2}$$

$$\cdot OH + CH_{4(gas)} \rightarrow CH_3OH \tag{3}$$

However, one of the main challenges for the practical application of the conversion of methane to methanol in PER-FC is the development of efficient, stable, and selective electrocatalysts. This kind of reactor can activate the water in the anode and promote the oxygen reduction reaction, as in a conventional fuel cell, and some electrical potential difference is established so that the reaction occurs spontaneously, and the electrical energy released can be used [3, 7].

Studies show that the use of palladium-based catalysts should significantly reduce the activation energy of CH_4, at its highest oxidation potential (Pd^{III}) [8]. In addition, many anodic catalysts based on transition metals, such as Ni, Cu, V, among others, are described in the literature for the conversion of methane [9–12]. The methane molecules can chemisorb on the surface of the catalysts and then form a

slightly polarized state. In addition, catalysts based on these transition metals favor the formation of active oxygen species, a fundamental requirement for the conversion of methane to methanol. In this sense, Ni-containing catalysts have attracted a lot of attention for the partial oxidation of methane by electrocatalysis. Many studies show excellent adsorption of methane on metallic Ni and NiO. Some reports report the oxidation ability of electrogenerated NiOOH to convert CH_4, while others focus on providing suitable oxidizing species for selective oxidation of CH_4 [13–15]. Nickel can be used in conjunction with other materials to produce a high catalytic performance for methane conversion.

On the other hand, the use of metallic oxides as a support can bring stability to the catalyst, since the reactive oxygenated species (ROS), responsible for the oxidation of methane in these devices, also act in the degradation of Vulcan carbon particles, which are usually used as supports for this process catalyst type [16, 17]. In this sense, we investigated the conversion of methane to methanol in a PER-FC using nickel-palladium anodic electrocatalysts in different atomic ratio using $Sb_5O{\cdot}SnO_2$ (ATO) support, because this oxide favors the formation of ROS, [18], it has good electrical conduction, corrosion resistance [19]. These characteristics make $SnO_2{\cdot}Sb_2O_5$ a great option for catalyst support for this reaction.

Experimental

The ATO-supported Pd and Ni-based materials were prepared by the sodium borohydride reduction method [20], that consist of a mixture of ultrapure water with isopropanol 50/50 (v/v) with an appropriate amount of support—ATO ($Sb_2O_5{\cdot}SnO_2$—Aldrich) was dispersed and later metallic precursors of $Pd(NO_3)_2{\cdot}2H_2O$ (Aldrich) and $NiCl_2{\cdot}2H_2O$ (Aldrich) of catalytic in order to obtain a load of 20% by mass of these metals in relation to the ATO. In this medium, $NaBH_4$ (Aldrich) was added in an aqueous solution with an excess of 5:1 in relation to the metals, and stirring was maintained for 30 min, after which time the material obtained was washed with ultrapure water and filtered.

The materials were characterized by X-ray diffraction, using a Rigaku X-ray diffractometer—Miniflex II, with a Cukα radiation source of 0.15406 Å. The diffractograms were obtained from 20° to 90°, with a scan speed of $2°min^{-1}$. The morphology was observed by transmission electron microscopy performed by a transmission electron microscope, JEOL JEM-2100, operated at 200 keV. For the construction of the histogram and the calculation of the average size, 300 nanoparticles of each catalyst were digitally mediated by microscopy.

The catalysts were further characterized by cyclic voltammetry performed in a three-electrode electrochemical cell in a PGStat 302 N Autolab potentiostat, with a working electrode built on a glassy carbon (0.2 cm^2) support covered with an ultra-thin porous layer, produced from a paint made with 8 mg of catalyst, 600 µL of ultrapure water, 400 µL of isopropanol and 15 µL of Nafion® (D-520) mixed in ultrasound, an Ag/AgCl 3.0 mol L^{-1} electrode used as a reference electrode and a 2 cm^2 Pt electrode used as a counter electrode. This same potentiostat and electrodes were used in conjunction with a Raman Macroram spectrometer—Horiba, with a

785 nm laser and an electrochemical cell suitable for carrying out the electrochemical assays assisted by in-situ Raman spectroscopy as reported by De Souza [21].

The conversion of methane to methanol was carried out in a PER-FC, with electrodes constructed with 1 mg of Pd + Ni per cm^2 at the anode, a membrane of Nafion 117 treated with KOH as electrolyte, and 1 mg of Pt/C—Basf (20% w/w) as the cathode. All electrodes were prepared by depositing the ink containing the catalyst with 30% by mass of a solution of Nafion D-520 (Aldrich) and isopropanol applied by brushing on a carbon cloth treated with PTFE. The reactor is based on a typical fuel cell coil plate design made in 316L steel, fed with a mixture of methane 100 mL min^{-1} and NaOH 1 mL min^{-1}, the ambient temperature at the anode, while the cathode is supplied with humidified O_2 in a bottle at a temperature of 85 °C with a flow rate of 400 ml min^{-1} at the cathode.

Aliquots of the reactor effluent are collected every 100 mV for 300 s from the open circuit potential to 0 V and analyzed by infrared spectroscopy performed on a Nicolett® 6700 with an ATR Miracle (Pike) accessory and diamond/ZnSe crystal and a detector of MCT, and high-performance liquid chromatography—HPLC (YL9100) with a UV/Vis detector with detection made at 205 nm, with flow of 0.8 ml min^{-1} of 50% water and 50% acetonitrile in an isocratic run on a C18 column (Phenomenex Luna 5 µm, 250 × 4.6 mm). The calibration curve presents the following linear equation: *peaks area* = 59.916 + 238.59 [*methanol*], and presenting $r^2 = 0.9981$.

Results and discussion

Figure 1a, b shows the X-ray diffraction patterns of palladium and nickel supported on ATO electrocatalysts. Intensive peaks are observed for all materials at 2θ to ~ 26º, 33º, 37º, 51º, 54º, 61º, and 64º, which corresponds to the support of the electrocatalysts, $Sn_2O{\cdot}Sb_2O_5$ (JCPDS# 88-2348). The sharpest and narrowest peaks are characteristic of the crystallographic planes (1 1 0) and (1 0 1) of the ATO. Based on the diffraction pattern with the intensity normalized by the logarithmic function, it was possible to observe more clearly the characteristic peaks of Pd, Ni, and the PdNi alloy. The Pd-related peaks at 2θ ~ 38º, 49º, 66º, and 81º are associated with the crystalline planes (111), (200), (220), (311) and (222) according to (JCPDS# 89-4897), reveals a face-centered cubic (FCC) structure. Furthermore, it can be observed that the position of the diffraction peaks of Pd–Ni undergoes a slight shift to an angle 2 θ smaller than that of Pd. This fact can occur when the Ni atom partially replaces the Pd position in the crystal lattice when the metal alloy is formed [22]. While the Ni/ATO catalysts show peaks at 2θ at 44, 57, and 78° corresponding to the Ni (JCPDS #87-0712) (111).

In addition, Fig. 1c showed the Raman spectra of the nanocatalysts Pd–Ni on ATO support. The Raman spectra present typical bands correspondent to the three fundamental active Raman vibration modes, E_g, A_{1g}, and B_{2g} near to 470, 636 and 775 cm^{-1}, respectively. These results showed a typical feature of the phase of SnO_2 according to the XRD patterns. It can be observed that the Pd–Ni inserted into ATO nanostructure led to a shift of these bands. Furthermore, the spectra region around

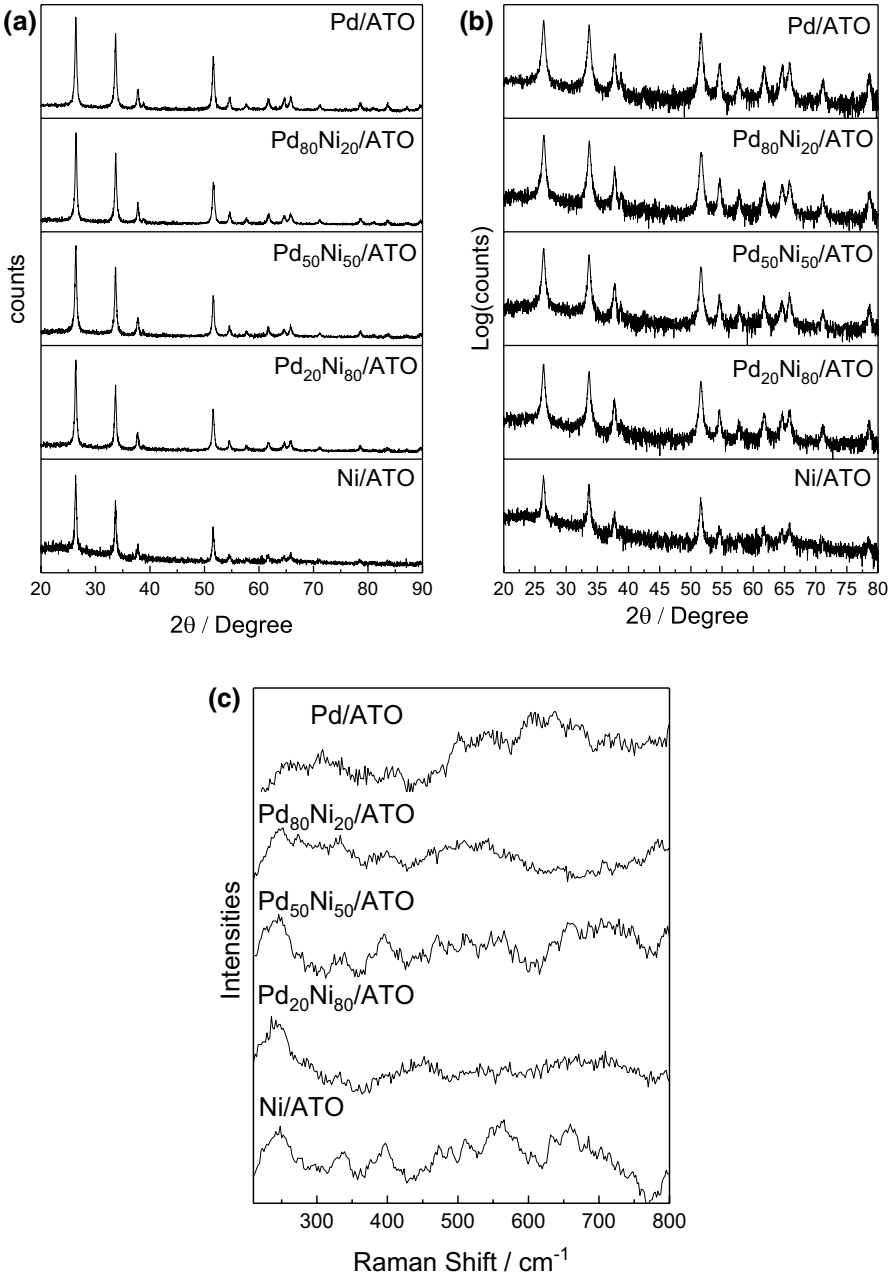

Fig. 1 **a** X ray diffractogram (XRD) pattern of the Pd and Ni catalysts supported on ATO; **b** logarithm of the intensities of the diffractograms in Fig. 1a. **c** Raman spectra of these materials

550–580 cm^{-1} indicates fingerprints of the SnO_2 structure's nano-size. At present, the addition of Ni in the materials can be the reason for the observation of the band in this region of the Raman spectra, due to the structure local disorder effect [23, 24].

The micrograph images of the Pd Ni-dopped on the ATO electrocatalyst are shown in Fig. 2 and their respective particle size histograms. The average measured

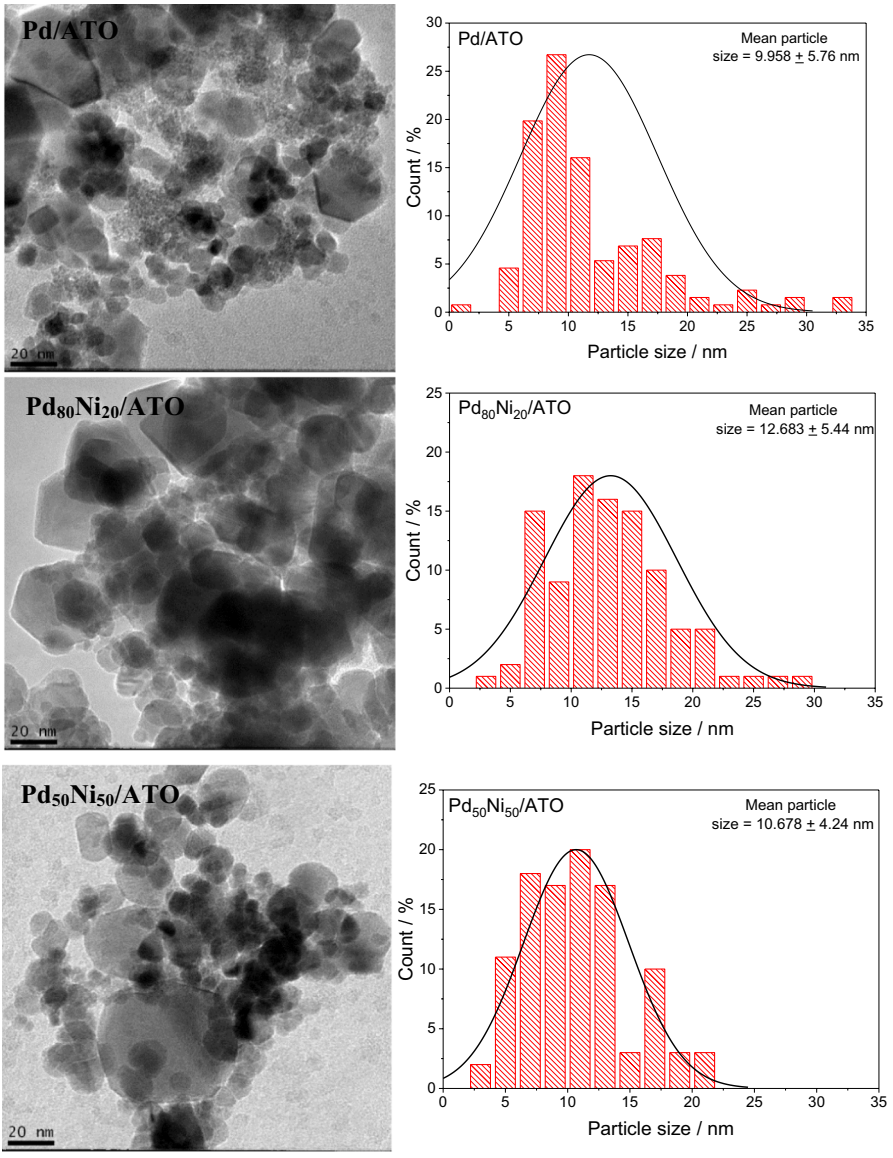

Fig. 2 TEM micrograph and histograms of the particle size distribution to Pd and Ni catalysts supported on ATO

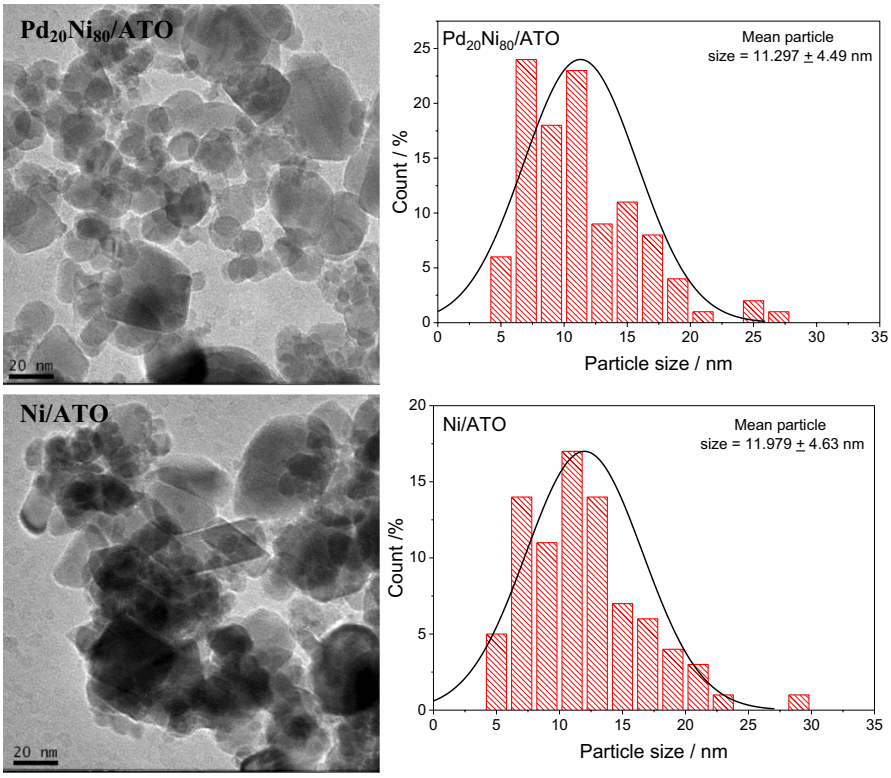

Fig. 2 (continued)

particle size of the nanoparticles ranges between 9 and 12 nm. It can be observed that the metallic nanoparticles are agglomerated under the surface of the ATO, which indicates that the support can favor agglomeration, which concerns the size of the particles. In addition, the average particle size is slightly larger than the carbon-supported PdNi metallic particles described by Santos (6–10 nm) [25].

The cyclic voltammetry (CV) is shown in Fig. 3 and describes the electrochemical properties of the Pd Ni-dopped/ATO catalysts. The results were obtained from the electrocatalysts with different compositions using NaOH 1.0 mol L^{-1} aqueous solution at room temperature and a sweep speed of 10 mV s^{-1}. The CV of the Pd/ATO electrocatalyst clearly indicates the current densities for hydrogen adsorption/desorption at − 0.85 and − 0.6 V, respectively. However, the peak definition is suppressed with the addition of Ni in the Pd nanostructure due to the synergistic effect of metallic oxides present, which can lead to a palladium surface [19]. The reduction of oxide to decrease with the higher proportion of Ni is a trend and in different perspectives of 0.05 V from $Pd_{80}Ni_{20}$/ATO, $Pd_{50}Ni_{50}$/ATO to $Pd_{20}Ni_{80}$/ATO, with the benefit of a higher proportion of Ni showing more potential. This fact can be explained by the stronger adsorption of oxide species on the surface of bimetallic materials due to the presence of Ni [26].

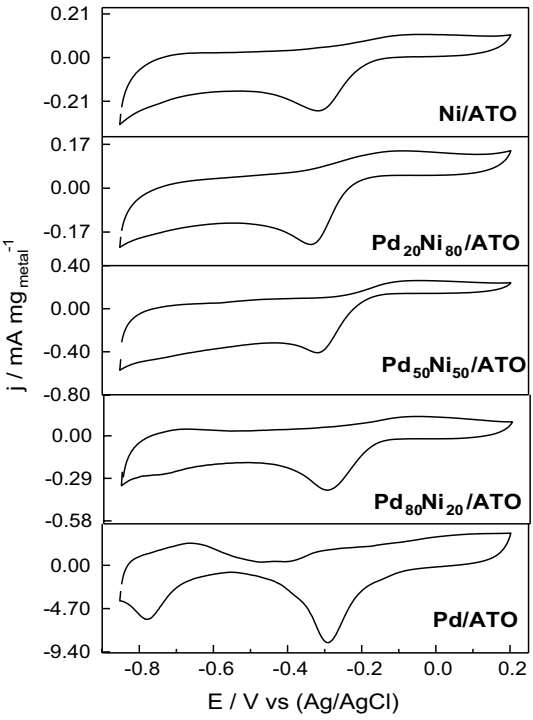

Fig. 3 Cyclic voltammetry curves of the PdNi on ATO electrodes in different proportions (scan rate $v = 10$ mV s^{-1}) in 1 mol L^{-1} NaOH aqueous solution

Analyses of the electrocatalytic activity in situ with Raman spectroscopy were performed to obtain more details of the processes that occur in the interaction of the catalyst with the electrolyte and the step of partial oxidation of methane, as shown in Fig. 4. In the spectra of all Pd Ni-dopped on ATO electrocatalysts, the characteristic bands of SnO_2 are observed at approximately 486, 602, and 780–793 cm^{-1}, referring to the active bands of SnO_2 E_g, A_{1g}, and B_{2g}, respectively [27, 28]. Furthermore, it is observed that there is a slight shift in the wavelength of these active bands because of Pd and Ni metallic nanoparticles. In addition, bands with wavelengths at 1314 and 1600 cm^{-1} are observed in materials containing Ni in their composition, indicating the presence of NiO [29], and these bands increase with the potential.

A band centered at 639 cm^{-1} corresponding to the bending of the PdO–H bond [30], indicating the oxidation of Pd as a function of potential, in the Pd/ATO catalyst, was convolved with the band at 602 cm^{-1} of SnO_2, and it is possible to see the bands at 794, 974, and 1166 cm^{-1} corresponding to Nafion [21].

The activities of Pd Ni-dopped on ATO electrocatalysts for the conversion of methane to methanol were analyzed in a PER-FC. In Fig. 5, observe the open circuit value presented by the electrocatalysts (OCV) that varies between 0.35 and 0.5 V values higher than that reported for materials supported on C [25, 31, 32]. This suggests that ATO support can act as a synergistic metallic Pd and Ni effect target higher potentials [3]. And the maximum power density was obtained for $Pd_{50}Ni_{50}$/ATO (0.37 mW cm^{-2}), about 20% bigger than Pd/ATO (0.30 mW cm^{-2}), the same composition that presents a higher power density than supported in carbon [25].

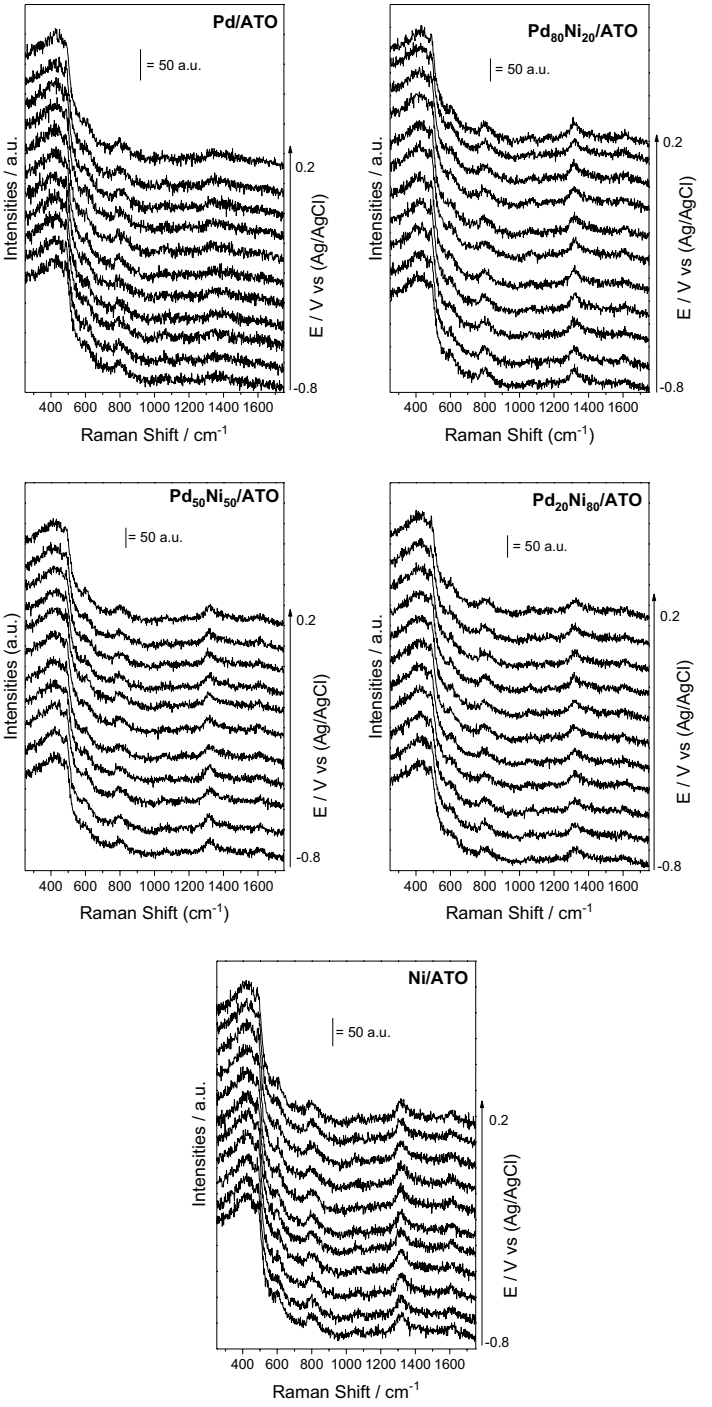

Fig. 4 Spectra of in-situ Raman-assisted electrochemical measurements collected at different potentials in NaOH 1.0 mol L^{-1}

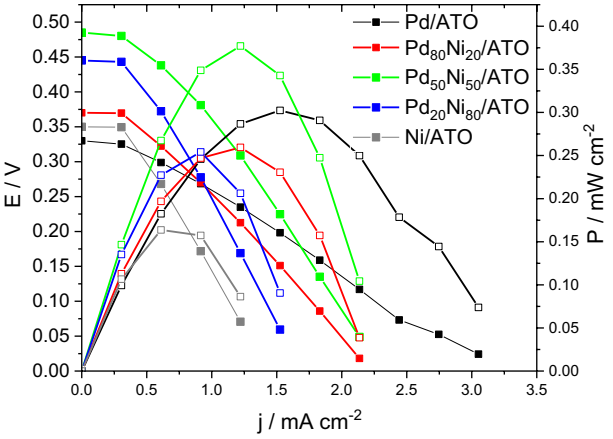

Fig. 5 The Polarization curves and the Power Density of a PdNi/ATO catalysts anode (5 mg cm^{-2} catalysts loading) and Pt/C Basf or the cathode in all experiments (1 mg Pt cm^{-2} catalyst loading with 20 wt% Pt loading on carbon), Nafion 117 membrane KOH treatment; NaOH 1.0 mol L^{-1} + CH_4 50 mL min^{-1}, and O_2 flux of 200 mL min^{-1}

To qualify the products formed during the operation of the Pd–Ni/ATO electrocatalysts in FC, the effluents were collected every 100 mV for 5 min. Each sample collected was analyzed by FT-IR spectroscopy and the graphs are plotted in Fig. 6. The spectra obtained show that for all effluents present a characteristic band of methane at ~ 1304 cm^{-1} [33, 34], this band appears near open circuit voltage (OCV) and increases with the potential decrease. Furthermore, the activities of partial oxidation of methane in the alkaline medium are such that, in addition to methanol, two other species, formate and carbonate, may form. Methanol has two characteristic bands, at 1034 and 1095 cm^{-1}, referring to the ν(C-O) stretching [9, 34] that are present in OCV until 0 V. The presence of formate and carbonate species can be confirmed by bands at wavelengths of approximately 1337 and 1395 cm^{-1}, respectively, and are characteristic of ν(COO) stretching [35, 36]. These species are detected for all electrocatalysts, including the Pd/ATO catalyst, the formation of a formate is observed as the potential increases.

The methanol produced was quantified by liquid chromatography and reported as a rate reaction according to Eq. (4) and the result is shown in Fig. 7, where it is possible to observe that the Pd/ATO composition is the most active for the conversion of methane into methanol at all potentials. Furthermore, other electrocatalysts show good activity to obtain methanol, but Pd/ATO is shown to be the second electrocatalyst to produce methanol at various potentials applied.

$$r = \frac{\text{Methanol}_{\text{amount}}}{\text{Volume} \times \text{Time}} \tag{4}$$

Figure 8 presents the dependence of the maximum power density (MPD) on Ni content, and this curve shows an optimal composition as observed by Santos et al. [25], and the maximum rate reaction accompanies the decrease of Pd.

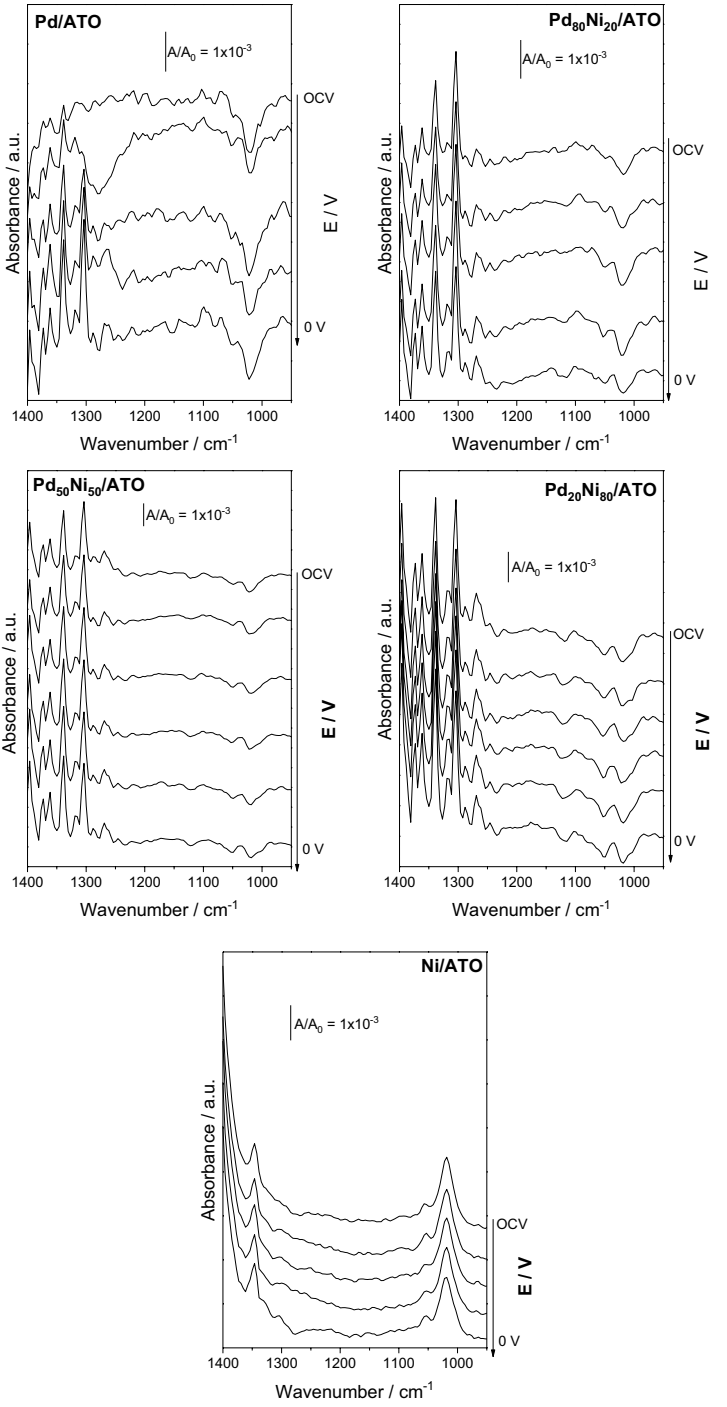

Fig. 6 FTIR spectra of the aliquots collected from the reactor effluent every 100 mV for 5 min in NaOH 1.0 mol L^{-1} with methane flow adjusted to 100 mL min^{-1} for all catalysts

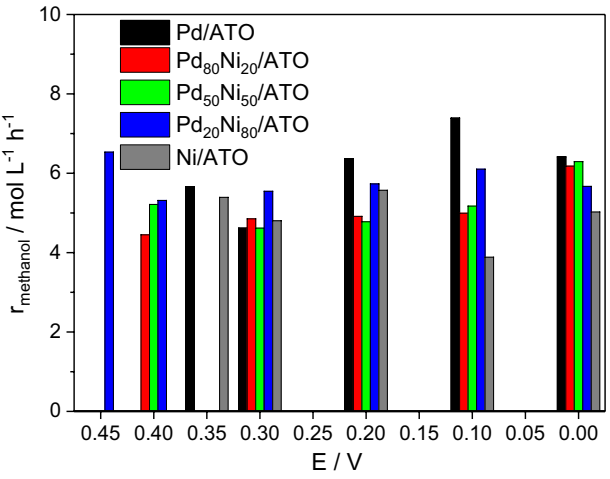

Fig. 7 Rate reaction of all Pd_xNi_y/ATO catalysts to methanol production

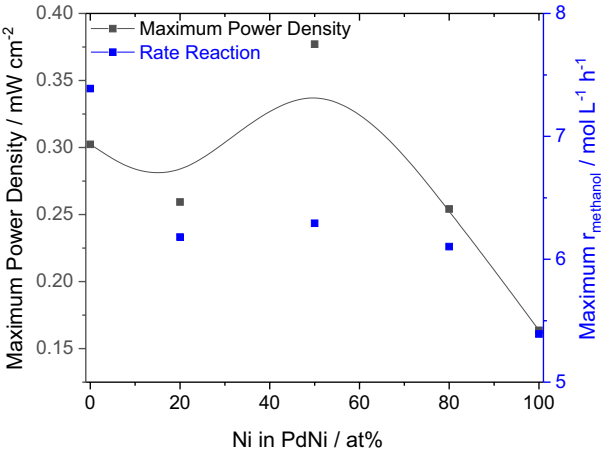

Fig. 8 Dependence of MDP and maximum rate reaction of methanol production on nickel content in PdNi/ATO catalysts

However, it is worth mentioning that for materials containing Pd and Ni the rate reaction is very close. Indicating that the $Pd_{50}Ni_{50}$ composition may be the most interesting for the co-generation of methanol and energy.

The insertion of transition metals such as Pd and Ni, and the metallic alloy PdNi in different compositions on the ATO surface showed promising results for the electrocatalytic conversion of methane to the methanol due the saving of palladium in the material and increasing the power obtained.

Conclusion

The ATO showed promise to be used as support for PdNi catalysts applied in the partial oxidation reaction of methane to methanol with co-generation of electrical energy. ATO as well as Ni activate water at low overpotentials providing reactive oxygen species for the reaction, and Pd as well as nickel also act as methane adsorption sites. The best proportion found was $Pd_{50}Ni_{50}$/ATO, even producing 20% less methanol than Pd/ATO. However, in compensation, it produces more than 20% more energy and uses 50% less noble metals.

Acknowledgements CAPES, CNPq (302709/2020-7), FAPESP (2017/11937-4) and CINE-SHELL (ANP) consented to the acknowledgement.

Authors' contributions JFC: Preparation of electrocatalysts, XRD and TEM experiments; planning and execution research. NGPF: Execution of The Polarization curves and the Power Density experiments IMG: Execution of Raman experiments. CMG: Execution of liquid chromatography experiments PVRG: Preparation, creation and/or presentation of the published work, specifically writing the initial draft. PJZ: Discussion of Raman and preparation and discussion of TEM experiments. RFBDS: reparation, creation and presentation of the published work writing the finally draft. Management and coordination for the research activity and execution and writing the finally draft. AON: Management and coordination responsibility for the research activity planning and execution; Oversight and leadership responsibility for the research activity planning and execution.

Funding This declaration is not applicable.

Availability of data and materials The datasets used can be accessed when requested.

Declarations

Competing interests This declaration is not applicable.

Ethical approval This declaration is not applicable.

References

1. C.-Y. Hung, A. VanderZaag, W. Smith, B. Grant, Sci. Total Environ. **835**, 155325 (2022)
2. H. Jiang, L. Zhang, Z. Han, Y. Tang, Y. Sun, P. Wan, Y. Chen, M.D. Argyle, M. Fan, Green Energy Environ. **6**, 1132 (2021)
3. R.F.B. de Souza, D.Z. Florio, E. Antolini, A.O. Neto, Catalysts **12**, 217 (2022)
4. A.S. Ramos, M.C.L. Santos, C.M. Godoi, A. Oliveira Neto, R.F.B. De Souza, ChemCatChem **12**, 4517 (2020)
5. R.L. Cook, A.F. Sammells, J. Electrochem. Soc. **137**, 2007 (1990)
6. L.M.S. Garcia, S. Rajak, K. Chair, C.M. Godoy, A.J. Silva, P.V.R. Gomes, E.A. Sanches, A.S. Ramos, R.F.B. De Souza, A. Duong, A.O. Neto, ACS Omega **5**, 16003 (2020)
7. T. Tagawa, K.K. Moe, M. Ito, S. Goto, Chem. Eng. Sci. **54**, 1553 (1999)
8. M.E. O'Reilly, R.S. Kim, S. Oh, Y. Surendranath, ACS Cent. Sci. **3**, 1174 (2017)
9. M.C.L. Santos, L.C. Nunes, L.M.G. Silva, A.S. Ramos, F.C. Fonseca, R.F.B. de Souza, A.O. Neto, ChemistrySelect **4**, 11430 (2019)
10. C.M. Godoi, M.C.L. Santos, A.J. Silva, T.L. Tagomori, A.S. Ramos, R.F.B. de Souza, A.O. Neto, Res. Chem. Intermed. **47**, 743 (2021)
11. J. Kang, E.D. Park, Catalyst **10**, 299 (2020)

12. R.S. Rocha, R.M. Reis, M.R.V. Lanza, R. Bertazzoli, Electrochim. Acta **87**, 606 (2013)
13. A. Antzara, E. Heracleous, L. Silvester, D.B. Bukur, A.A. Lemonidou, Catal. Today **272**, 32 (2016)
14. S. Wang, T. Itoh, T. Fujimori, M.M. de Castro, A. Silvestre-Albero, F. Rodríguez-Reinoso, T. Ohba, H. Kanoh, M. Endo, K. Kaneko, Langmuir **28**, 7564 (2012)
15. M. Jafarian, M.G. Mahjani, H. Heli, F. Gobal, M. Heydarpoor, Electrochem. Commun. **5**, 184 (2003)
16. A. Bekisch, K. Skadell, D. Poppitz, M. Schulz, R. Weidl, M. Stelter, J. Electrochem. Soc. **167**, 144502 (2020)
17. S. von Kraemer, K. Wikander, G. Lindbergh, A. Lundblad, A.E.C. Palmqvist, J. Power Sources **180**, 185 (2008)
18. L. Sun, Z. Liu, Y. Bao, H. Li, W. Bao, Int. J. Mater. Res. **105**, 584 (2014)
19. W. Qu, Z. Wang, X. Sui, D. Gu, Int. J. Hydrog. Energy **39**, 5678 (2014)
20. J. Nandenha, R.F.B. De Souza, M.H.M.T. Assumpcao, E.V. Spinace, A.O. Neto, Ionics **19**, 1207 (2013)
21. R.F.B. De Souza, É.T. Neto, M.L. Calegaro, E.A. Santos, H.S. Martinho, M.C. dos Santos, Electrocatalysis **2**, 28 (2011)
22. G. Wang, D. Li, Y. Zuo, Y. Tang, X. Zhang, X. Zhao, Coatings **10**, 161 (2020)
23. I.M. Costa, Y.N. Colmenares, P.S. Pizani, E.R. Leite, A.J. Chiquito, Chem. Phys. Lett. **695**, 125 (2018)
24. B.C. Bhadrapriya, A.R. Varghese, G. Amarendra, S. Hussain, Sb:SnO2 thin films-synthesis and characterization, in *AIP Conference Proceedings*, vol. 1951 (2018), p. 030006
25. M.C.L. Santos, C.M. Godoi, H.S. Kang, R.F.B. de Souza, A.S. Ramos, E. Antolini, A.O. Neto, J. Colloid Interface Sci. **578**, 390 (2020)
26. M.D. Obradović, Z.M. Stančić, U.Č Lačnjevac, V.V. Radmilović, A. Gavrilović-Wohlmuther, V.R. Radmilović, S.L. Gojković, Appl. Catal. B **189**, 110 (2016)
27. F.H. Aragón, J.A.H. Coaquira, P. Hidalgo, S.W. da Silva, S.L.M. Brito, D. Gouvêa, P.C. Morais, J. Raman Spectrosc. **42**, 1081 (2011)
28. A. Leonardy, W.-Z. Hung, D.-S. Tsai, C.-C. Chou, Y.-S. Huang, Cryst. Growth Des. **9**, 3958 (2009)
29. N. Mironova-Ulmane, A. Kuzmin, I. Steins, J. Grabis, I. Sildos, M. Pärs, J. Phys. Conf. Ser. **93**, 012039 (2007)
30. M. Muniz-Miranda, A. Zoppi, F. Muniz-Miranda, N. Calisi, Coatings **10**, 207 (2020)
31. J. Nandenha, I. Nagahama, J. Yamashita, E. Fontes, J. Ayoub, R. de Souza, F. Fonseca, A. Neto, Int. J. Electrochem. Sci. **14**, 10819 (2019)
32. J. Nandenha, E.H. Fontes, R.M. Piasentin, F.C. Fonseca, A.O. Neto, J. Fuel Chem. Technol. **46**, 1137 (2018)
33. D. Scarano, S. Bertarione, G. Spoto, A. Zecchina, C. Otero Areán, Thin Solid Films **400**, 50 (2001)
34. J. Nandenha, R.M. Piasentin, L.M.G. Silva, E.H. Fontes, A.O. Neto, R.F.B. de Souza, Ionics **25**, 5077 (2019)
35. P.A. Christensen, D. Linares-Moya, J. Phys Chem. C **114**, 1094 (2010)
36. X. Fang, L. Wang, P.K. Shen, G. Cui, C. Bianchini, J. Power Sources **195**, 1375 (2010)